J Mater Sci (2007) 42:7299–7306
DOI 10.1007/s10853-007-1585-y

Microstructure-microhardness relationships in friction stir welded AA5251

Moataz M. Attallah · Claire L. Davis · Martin Strangwood

Received: 10 May 2006 / Accepted: 6 February 2007 / Published online: 10 May 2007

Abstract Quantitative microstructural studies using optical and electron microscopy were carried out to determine the grain size and intermetallic particle distributions in various locations of friction stir welds in AA5251 to study their influence on the microhardness. Grain-boundary strengthening, (using Hall-Petch relation) was found to be the dominant factor controlling weld hardness within the thermomechanically-affected zone (TMAZ), yet with a minor increase in the Hall-Petch intercept from the Al–Mg alloys literature values. This deviation was associated with solid-solution strengthening resulting from the dissolution of Mg_2Si particles during welding. A contribution from precipitate strengthening accounted for deviations from the overall Hall-Petch relationship. This was linked to the formation of submicron $Al_6(Fe,Mn)$ particles observed within the TMAZ grains, varying in density with position in the weld, and accordingly their strength contribution. Differential Scanning Calorimetry (DSC) was used to quantify the strengthening contribution of the dislocation stored energy in the TMAZ of the weld. Although significant stored energy was detected, this was mostly due to the presence of geometrically-necessary (non-strengthening) dislocations and did not contribute to hardness.

M. M. Attallah · C. L. Davis · M. Strangwood
Department of Materials and Metallurgy, The University of Birmingham, Elms Road, off Pritchatts Road, Edgbaston, Birmingham B15 2TT, UK

C. L. Davis
e-mail: c.l.davis@bham.ac.uk

M. Strangwood
e-mail: m.strangwood@bham.ac.uk

Present Address:
M. M. Attallah (✉)
University of Manchester Materials Science Centre, Manchester M1 7HS, UK
e-mail: m.attallah@hotmail.co.uk

Introduction

Friction Stir Welding (FSWing) is a solid-state joining process in which joining takes place through a combination of frictional heating and plastic deformation by stirring [1]. The maximum temperature measured during FSWing of Al-based alloys falls between $0.7T_m$ and $0.9T_m$ [2], which can thus classify FSWing as a hot working process. Hot working processes are usually associated with recrystallisation, forming new strain-free grains (dislocation density in the range of 10^8–10^{10} dislocations/m^2), provided that the thermal activation and driving force are sufficient [3].

During FSWing, a major component of the total energy is dissipated as heat, and a small component is retained within the deformed microstructure as stored energy, due to point defects, boundaries and particularly dislocations [4]. Establishing structure-property relationships for FSWs of age-hardenable Al-based alloys, is relatively simple since the precipitate distribution within the weld (and accordingly the strength) depends on the thermal fields generated by the tool [5, 6], which can be readily modelled. However, for work hardenable Al-based alloys, the complex microstructural development associated with FSWing (e.g., dislocation structure [7], grain refinement by dynamic recrystallisation [8], particle break-up or fragmentation-assisted particle dissolution [9–11]), makes establishing structure-property relationships more difficult. There has been an ongoing discussion regarding the main factors that

control the FSW strength in work hardenable Al-alloys [12–17]. For example, the strength in AA5xxx FSWs has diversely been attributed to the grain size [15–17], the extent of the thermally-dissolved Mg solute atom concentration which increases the strength by dislocation-blocking [16], and finally the influence of the fragmented submicron dispersoids that block dislocation movement (dislocation looping, Orowan hardening) [14]. However, these studies generally conclude that the influence of dislocation density, which has not been quantified, causes a discrepancy between the predicted and measured strength levels in the weld.

There has been recent progress in utilising Differential Scanning Calorimetry (DSC) to indirectly determine the dislocation density by measuring the release of stored energy [4, 18–20], which provides a feasible and simple technique when compared to transmission electron microscopy (TEM). The dislocation density (ρ) is related to the released stored energy per unit volume (E) through [4, 20]:

$$E = \rho \alpha G b^2 \quad (1)$$

where α is a dimensionless dislocation interaction parameter, G is the shear modulus, and b is the Burger's vector. In this paper, DSC measurements are used to provide an approximation for the extent of the dislocation-stored energy in the thermomechanically-affected zone (TMAZ), which is combined with microstructural quantification in order to account for hardness (and hence strength) variations through an Al–Mg FSW.

Experimental

The base material used in this study was AA5251 5 mm thick sheets. The chemical composition of the alloy is shown in Table 1. FSWing was carried out on fully-annealed (O) and work-hardened to half-hard and stabilised (H34) conditions. The welding parameters were a rotation speed of 500 rpm and traverse speed of 500 mm/min.

DSC thermal analysis was performed in a DSC 404C Pegasus® calorimeter. Small specimens (~3.5 × 2.5 × 1.5 mm, ~35 mg) were cut from the weld transverse cross-section as shown in Fig. 1 using a low-speed SiC cutting disc. A block of fully annealed commercially pure Al-alloy (99.5%) or 5251-O, of virtually the same mass as the specimen, was used as a reference. The latter provides a reference of matching temperature-dependent thermal properties. Specimens and references were thermally cycled for two runs [18], in fully recrystallised Al_2O_3 pans in a flowing Ar atmosphere at a heating rate of 20 °C/min. After the first run, the calorimeter was left to cool down without removing the sample, the second run (being linear indicating no transformations taking place) was used as a baseline as shown in Fig. 2. Quantification of the exothermic peak characteristics (start, end, energy release) was performed using Proteus-NETZSCH software. Interrupted thermal cycles (to peak temperatures of 375°, 400°, 475°, and 525 °C), using the DSC heating rate followed by cold water quenching, were carried out on base metal and full weld specimens using a Gleeble 3500 thermomechanical simulator.

Transverse sections, cut as above, were mounted, ground and polished to a 0.04 μm colloidal-silica suspension finish. A two-stage etchant, based on Weck's reagent, was used to reveal the grain structure of the recrystallised weld nugget (WN). The specimen was first immersed in a 2 g NaOH in 100 ml distilled water solution for ~30 s. After rinsing in distilled water and drying, the specimen was immersed in a 4 g $KMnO_4$, 1 g NaOH, 100 ml distilled water solution for ~10–15 s. The resulting structures were observed optically using a Leica DMRX microscope equipped with KS300 image analysis software. The latter software was used to determine grain size (equivalent circle diameter) from six fields at 1 mm spacing within the labelled dashed black boxes in Fig. 1 as well as intermetallic particle equivalent diameter and area fraction. Gleeble specimens were prepared and analysed in a similar manner.

Vickers hardness testing was carried out on polished specimens using a Mitutoyo microhardness tester, with a 2-axes micrometer-controlled stage to define the exact position relative to the surface, using a 1 kg load. Hardness traces were taken at depths of 1.5 mm and 3.5 mm from the weld surface, covering ±20 mm from the weld centreline, with 1 mm spacing between the indentations. Average values for hardness within the specified locations of the weld (as the WNU, WND, AS and RS regions in Fig. 1) were obtained by taking at least eight measurements within the dashed black boxes in Fig. 1, yet keeping the spacing between the indentations at 2–5 times larger than the diagonal of the indentation.

For TEM, specimens were prepared by spark-eroding 3 mm discs from the weld face as shown in Fig. 1. The discs were mechanically ground, electro-polished, and

Table 1 Chemical composition of AA 5251 used in this study (wt.%)

	Mg	Mn	Cr	Cu	Fe	Si	Ti	Zn	Al
Measured	1.94	0.35	0.11	0.1	0.5	0.32	0.03	0.06	Bal

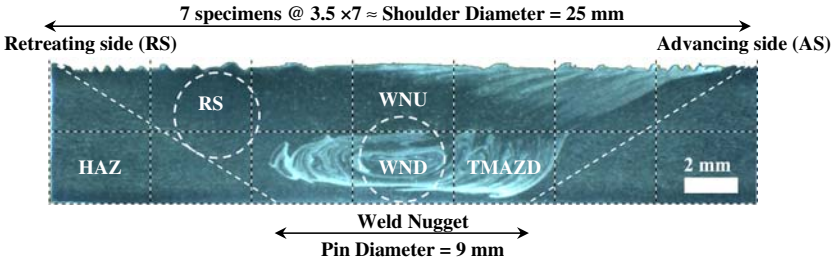

Fig. 1 Section through the FSW (slightly etched in 10% H_3PO_4 solution) showing where DSC specimens were taken from (dashed black boxes) and selected notation (U 'upper' half of sheet and D 'down' or bottom half of sheet). The white dashed circles show the location of the TEM specimens

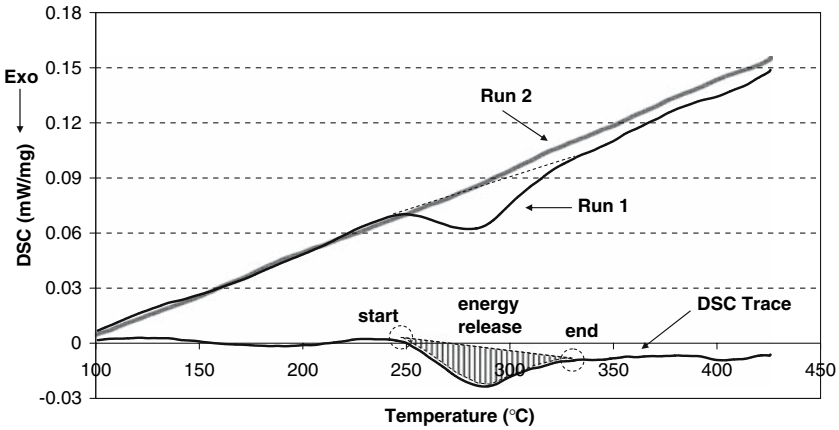

Fig. 2 The two-run approach used in measuring the stored energy

investigated in a Philips CM20 TEM operating at 200 kV. The KS300 image analysis software was again used to measure grain and particle equivalent diameter, and particle area fraction from TEM micrographs.

Results and discussion

FSWs are typically composed of a WN, a TMAZ, and a heat affected zone (HAZ). The WN is the region previously occupied by the tool pin and is generally considered to be part of the TMAZ. The TMAZ is the trapezoidal region whose bases are the shoulder diameter and the pin diameter at the bottom as shown in Fig. 1. The TMAZ contains dynamically recrystallised and plastically deformed grains. Beyond the TMAZ, the HAZ exists, which is only thermally affected. Other features include concentric ellipses within the WN, generally at the bottom (lower half) of the sheet, referred to as onion rings [12]. FSWs are asymmetric; whereby the side where the traverse speed and the tangential velocity component of the rotating tool are in the same direction is called the advancing side (AS), while the other side is called the retreating side (RS). The TMAZ/HAZ boundary towards the AS is sharper, compared to a more diffuse boundary towards the RS.

By looking into the hardness traces obtained for the H34-FSW and O-FSW conditions (Fig. 3), taken at 1.5 mm (up) and 3.5 mm (down) from the weld surface (Fig. 1), it is possible to link the macrostructural regions to the hardness. For the 'up' trace, the highest hardness (~72–74 Hv) was found at the AS, with the hardness decreasing towards the RS reaching a minimum of 50–55 Hv at the TMAZ/HAZ boundary. Then, within the HAZ the hardness increases in the H34-FSW gradually with the fading out of the thermal field experienced during welding, or decreases gradually in the O-FSW until it reaches the O-base metal hardness (54 ± 2 Hv). For both the O and H34 base metal conditions, the 'up' hardness traces exhibit similar features, i.e., a hardness around 55 Hv at the RS extending through to the centreline (fluctuation between 50 Hv and 60 Hv is seen with the O-base metal, Fig. 3b) followed by a rise to a peak of 70–75 Hv on the AS. This suggests that the structure developed during FSWing in the TMAZ on the AS has a stronger effect on hardness than the starting structure, which appears to have greater influence towards the RS. The 'down' traces also show similar trends for both welds with the peak hardness being recorded along the weld centreline in both cases. In the H34 FSW, the hardness through the onion rings region of the WN (±4.5 mm from the weld centreline along the 'down' traces) was relatively constant, before decreasing sharply towards a minimum in the HAZ. The overall behaviour was similar for the O base metal, although the hardness decreased across the onion rings region before decreasing sharply into the HAZ. These profiles differ from many traces reported for FSWs of work-hardened and annealed tempers (e.g., [12]), but the variations noted above indicate that the hardness throughout different weld regions results from a

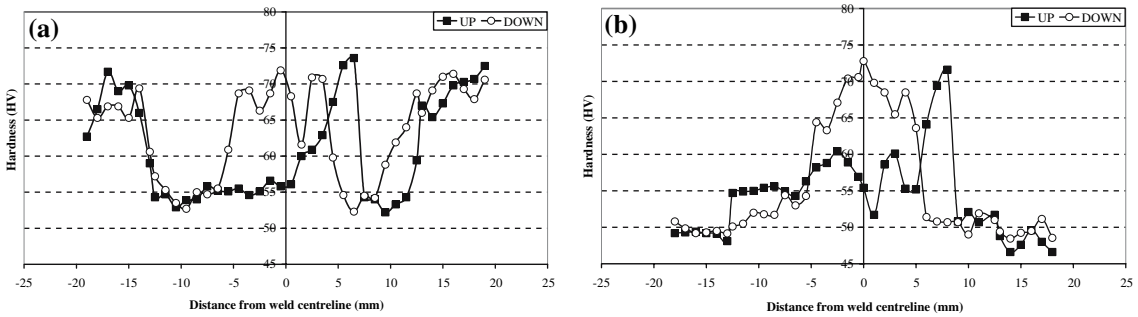

Fig. 3 Hardness traces for (**a**) the H34-FSW and (**b**) the O-FSW taken at 1.5 mm (up) and 3.5 mm (down) from the surface (the AS of the weld is to the right in each graph)

combination of the base metal and the structural modification during welding. Hence, more detailed characterisation was undertaken to explain the trends in hardness.

Grain size

To establish the grain size strengthening effects, thermal simulations for the H34 base metal to temperatures of 375, 400, 475, and 525 °C (i.e., after full recrystallisation, determined from DSC measurements) were carried out to establish a Hall-Petch relationship. It was found that grain growth caused a decrease in strength for heat treatments to 375, 400 and 475 °C however at 525 °C an increase in strength of ~4 Hv was seen which is consistent with dissolution of Mg_2Si, enriching the Mg-content in solid solution [21], as shown in Fig. 4.

The three specimens cycled at 375, 400, and 475 °C were fitted to a Hall-Petch-based relation given by: $Hv = 43 + 44d^{-1/2}$ as shown in Fig. 5. Based on the structure-property work of Furukawa et al. on Al-Mg alloys [22], and assuming a linear relationship between the Hall-Petch slope and intercept, and the Mg content of the alloy, the Hall-Petch relation for 5251 can be estimated at: $Hv = 38 + 45d^{-1/2}$, which is close to the one calculated for the investigated alloy. Possible reasons for the difference between the calculated relation and the one estimated from the literature (especially the intercept value) can be related to differences in other alloying elements (e.g., the extent of Mg or Mn in solid solution) and varying amounts of constituent particles.

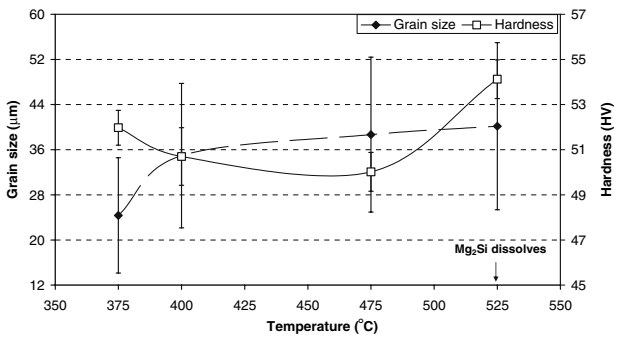

Fig. 4 Grain size and hardness development for the H34-base metal specimens thermally cycled at 20 °C/min to peak temperature then quenched

Microstructural quantification was carried out to relate to microhardness values for the various regions indicated in Fig. 1. Hence, the average grain sizes were determined for these regions rather than any variation within them. These average values are summarised in Table 2, and indicate that the finest grain size existed towards the AS below the weld surface, and increasing towards the RS.

This grain size trend is at variance with some previously published data (e.g., [23]), but the grain size is determined by a variety of factors including base metal condition, process parameters and tool design. Within this study the development of grain size has not been fully characterised to explain the differences with the previously published trends, which is the subject of a separate study. Figure 5 shows that the grain size effect on hardness accounts for the high hardness values seen in the WNU and RS of the TMAZ. However the WND and AS show higher hardness values than would be predicted by grain size alone. A WNU specimen was thermally-cycled in the Gleeble to 375 °C at 20 °C/min (complete recrystallisation) to study the change in strength due to the change in grain size. Yet, the hardness still did not change despite the change in grain size and annealing (stored energy release). It can be inferred from the Hall-Petch

Table 2 Grain size data for the various regions in the weld

Region	Average grain size (μm)	Standard deviation
WNU	5.69	0.67
WND	6.40	1.05
TMAZ-AS	3.69	0.23
TMAZ-RS	6.57	1.23

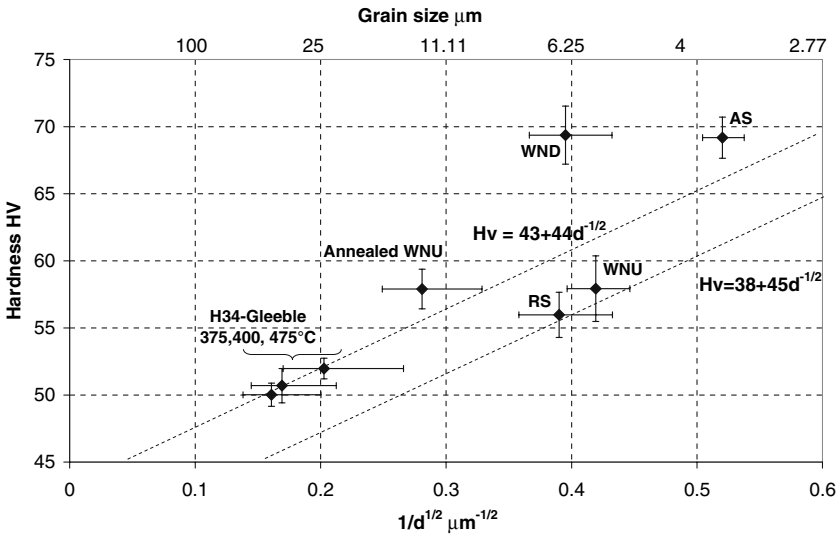

Fig. 5 Hall-Petch plot showing the contribution of the grain size to hardness for some of the FSW positions. Error bars are based on the standard deviation in measured hardness and grain size values

plot that there are two Hall-Petch relations; a lower one which includes RS and WNU points from the weld which rely mainly on grain size strengthening, and the upper one which includes the Gleeble-cycled base metal and WNU. Due to the relatively long thermal exposure, the upper limit relation may be influenced by the dissolution of particles, such as Mg_2Si, in addition to grain size strengthening, as opposed to the weld specimens that experienced similar transient thermal cycles. Thus, this may slightly increase their hardness as will be discussed in Sect. ''Other strengthening factors''. The Gleeble-cycled WNU has an even higher hardness due to the superposition of the thermal-stirring effect during welding followed by further thermal cycling. Still, both the AS and WND points from the weld seem even higher than the upper-limit relation by about 4–8 Hv. Hence there is a need to quantitatively consider the other factors that contribute to the FSW hardness, such as the stored energy, solid solution and particle strengthening.

Stored energy

In Fig. 6, the DSC trace for the 'H34' base metal is plotted alongside the traces for a section extracted from the WN base (WND) and a neighbouring specimen from the TMAZ. Compared to the base metal, specimens in both conditions extracted from the TMAZ (including the weld nugget) showed an exothermic peak corresponding to re-crystallisation between 240 °C and 330 °C (compared with 320 °C and 385 °C in the 'H34' base metal). This is attributed to the fact that recrystallisation depends on the amount of pre-deformation and grain size. The higher the extent of deformation, the higher is the tendency of the material to undergo recrystallisation at a lower temperature than the normal recrystallisation temperature [4, 20]. Low-energy peaks (<0.1 J/g) were frequently observed for TMAZ and WN samples between ~160 °C and ~190 °C, or between ~340 °C and ~360 °C which correspond to recovery and grain growth respectively. Both the single-run

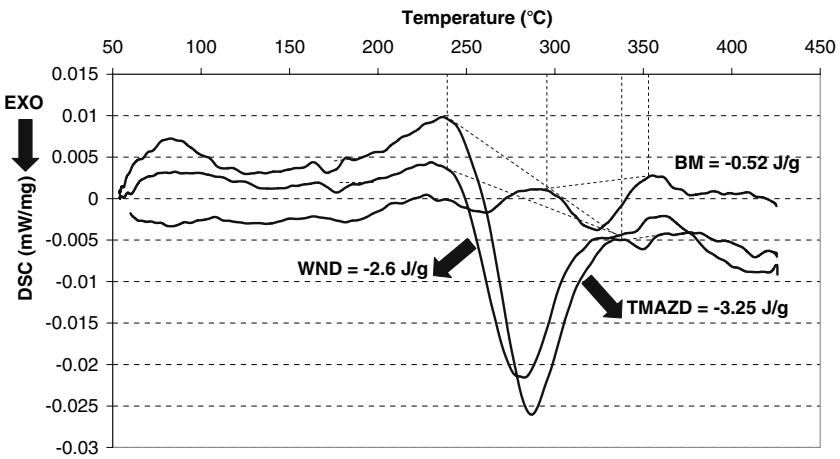

Fig. 6 DSC scans for the H34-base metal, compared to selected locations from the H34-FSW according to the notation in Fig. 1 and the amount of energy release and temperature range

as well as the double-run traces were compared to determine the position of the peaks.

The spatial variation in the extent of stored energy within specimens extracted from the weld (only covering the tool shoulder width) is shown in Fig. 7. The energy levels in the WNU and WND specimens were ~–2.5 J/g for both the O-FSW and H34-FSW conditions, which suggests that this region has experienced a similar amount of thermo-mechanical exposure. This also indicates that the dynamic recrystallisation processes and dislocation formation were dominant irrespective of the starting base material condition. The distribution also shows that the maximum stored energy was observed at the AS regardless of the starting condition (–3.65 J/g and –3.72 J/g for the O and H34 conditions respectively).

In Sect. ''Grain size'' it was shown that the RS and WNU hardness values were predicted well by considering grain size strengthening. However, the WND and AS were not well predicted, with the experimental values being greater than that predicted by grain size alone. It can be seen from Fig. 7 that the stored energy in the WNU and WND are virtually the same (≈–2.5 J/g) whereas the stored energy in WNU and RS are different (–2.5 J/g and <–1 J/g for the H34 condition).

To obtain an estimate for the dislocation density in the weld based on the stored energy release in the DSC, equation [1] can be used, which gives $\rho_{\text{dislocation}}$ ~6.2×10^{15} m^{-2} corresponding to an energy release of –2.5 J/g using $\alpha = 0.5$ (which is a typical literature value [4]), and gives $\rho_{\text{dislocation}}$ ~1.3×10^{15} m^{-2} for an energy release of –0.5 J/g in the case of the base metal (H34). The dislocation density in the base metal, as estimated by the DSC, is comparable to the values measured in a cold-rolled Al–Mg–Cu–Mn alloy using a combination of TEM and electron backscattered diffraction [24].

Several models have been used in an attempt to explain the dislocation density development in deformed materials and its influence on strength. In Ashby's strength model

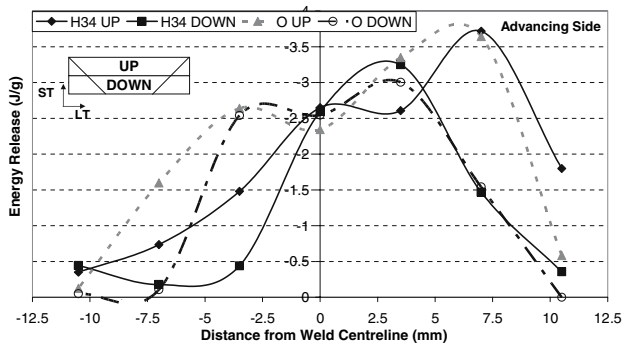

Fig. 7 Variation in energy release (stored energy) at different locations within the weld

[25], it is suggested that the total stored dislocations are divided into two types: *statistically stored dislocations* (ρ_S), which occur within the grains independent of any constraints imposed by the grain boundaries, and *geometrically-necessary dislocations* (ρ_G) which are created due to constraints imposed by the grain boundaries, non-deformable particles, and the plastic shear strain (γ), and are thus dependent on the grain size (d) and non-deformable particle distribution. This model shows that any work hardening effects are entirely due to ρ_S. Thus, since dynamic recrystallisation takes place during FSWing within the TMAZ, it can be expected that the influence of ρ_S becomes reduced compared to the influence of ρ_G. Using Ashby's model, ρ_G, due to the strain incompatibility caused by the solid solution matrix grains, can be estimated using:

$$\rho_G = 4\gamma/b\lambda \tag{3}$$

where λ is the geometric slip distance, which is assumed to be the grain size in pure, polycrystalline materials.

There will also be a contribution to ρ_G from the non-deformable particles (e.g., Al(FeMn)Si particles in Al-alloys), which, for an area fraction F_v and particle size r, is given by:

$$\rho_G = 3F_v\gamma/rb \tag{4}$$

where the total ρ_G is the sum of the contributions from Eqs. (3) and (4).

As indicated in the literature [4, 25], these relations have only been studied for low-strains. However, there is evidence that the strain incompatibility due to the existence of non-deformable constituent particles or the grains will increase the dislocation density of the material. For large strains, the influence of dynamic recovery may reduce the dislocation density from that predicted by Ashby's model. Estimates for the shear strain in the WN of a FSW vary between 10 and 20 [26]; using the lower strain value for the WN of the welds in this study with Al(FeMn)Si constituent particles ($F_v = 0.02$, $r = 0.5$ μm) and an average grain size of 6 μm, gives a total ρ_G value of 3.9×10^{16} m^{-2}. This compares with a total dislocation density of 6.2×10^{15} m^{-2} calculated using equation [1] (for $\alpha = 0.5$) from DSC measurements. Thus, for the plastic strains experienced in the WN to be retained after dynamic recovery, the sum of the geometrically-necessary contributions dominates the measured stored energy.

Therefore, despite the energy stored in dislocations in the weld, these dislocations do not seem to contribute much to the weld strength since it is mainly due to the geometrically-necessary dislocations. Therefore, to explain the strength of WND or AS, it is important to consider the

other strengthening factors, which are solid solution and particle strengthening.

Other strengthening factors

There are two additional strengthening factors to be considered: solid solution strengthening, which could be influenced by both the Mg and Mn content in solid solution, and particle (Orowan) strengthening by fine particles that precipitate during welding.

Depending on their size and solidus temperature, Mg_2Si particles were found to experience spatially heterogeneous dissolution; the area fraction of Mg_2Si ranging between 0.001 and 0.003 within the TMAZ compared to 0.005 in the base metal, which accordingly alters the solid solution levels [9]. The dissolution of Mg_2Si increases the Mg content in solid solution, which increases the strength through dislocation-solute atom interaction. If the Mg_2Si particles completely dissolve, they are expected to produce a strengthening contribution of about ~4 Hv corresponding to an increase of ~0.25 wt.% Mg.

Moreover, it was reported that during the thermal cycle of the weld precipitation of $Al_6(Fe,Mn)$ particles takes place within the WN [14, 27]. As shown in Fig. 8, precipitation of $Al_6(Fe,Mn)$ was evident in the WND to an area fraction of around 0.025, whereas the average size (equivalent radius) was found to be ~100 nm. TEM imaging of specimens from the RS failed to reveal such a level of precipitation. The small particles in WND can increase the strength through Orowan hardening, which is given as:

$$\tau = Gb/l \tag{5}$$

where l is the interparticle spacing, which is given as a function of the particle fraction F_V and radius r:

$$l = (2\pi/3F_V)^{1/2} r \tag{6}$$

This estimates the contribution of Orowan strengthening to correspond to about ~8 Hv. This agrees with the estimate of Sato et al. [14] of the contribution of Orowan hardening in a 5083-FSW to be ~10 Hv. It would be difficult to quantify this influence throughout the weld as this can only be done using the TEM, but this estimate accounts for approximately half the Hv difference between WND and WNU/RS, Fig. 5.

Thus, it appears that the weld strength depends mainly on two structural factors: grain-size and particle strengthening with increased solid solution strengthening from soludle particle dissolution having a secondary effect. The complex microstructural development associated with FSWing divides the weld into regions which depend primarily on grain boundary strengthening and other regions that depend on grain boundary and particle strengthening. Despite the high dislocation density within the weld, these provide insignificant contribution to the weld strength compared to grain and particle strengthening. Whilst increased solid solution strengthening might be significant in other weld systems, for the system studied here the extent of dissolution of Mg_2Si particles gives increased hardening by about 4 Hv only.

Conclusions

The influence of the various microstructural strengthening factors on the hardness in AA5251 FSWs was studied. After distinguishing the various influences, it was found that the TMAZ/WN strength was found to be primarily controlled by grain boundary strengthening and, in specific locations by dislocation-particle (Orowan) strengthening caused by the submicron $Al_6(Fe,Mn)$ particles. Despite the high dislocation stored energy measured in the TMAZ/WN compared to the base metal, the high stored energy was associated mainly with geometrically-necessary (non-strengthening) dislocations resulting from the grain

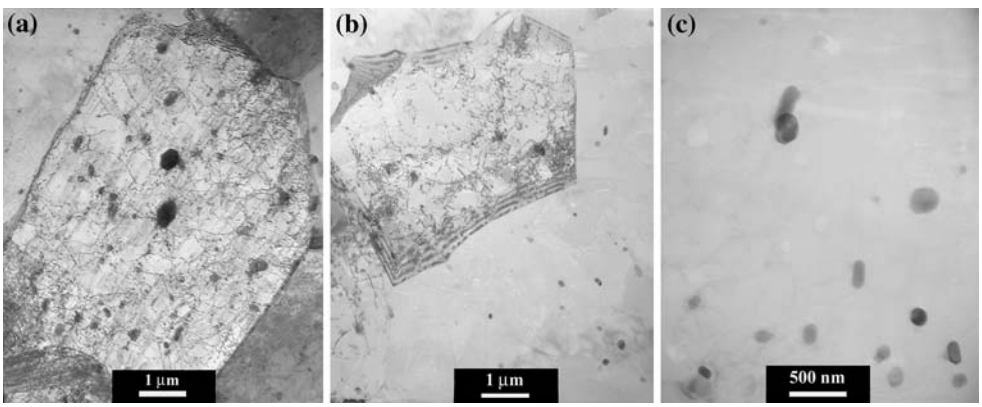

Fig. 8 TEM micrographs from the weld showing the precipitation of the Al6 (Fe, Mn) particles in: (**a**) Weld nugget (down), (**b**) Retreating side, (**c**) Particles in the weld nugget down

refinement and presence of intermetallic particles as a result of the large strain deformation during FSW.

Acknowledgements The support of TWI Ltd. for this research is acknowledged. One of the authors (MMA) would like to acknowledge the financial support of the Department of Metallurgy and Materials at the University of Birmingham and the Overseas Research Scholarship provided by Universities-UK.

References

1. Thomas WM, Nicholas ED, Needham JC, Nurch MG, Templesmith P, Dawes C (1991) International Patent Application No. PCT/GB92/02203 and GB Patent Application No. 9125978.8, Dec. 6
2. Tang W, Guo X, McClure JC, Murr LE (1998) J Mater Process Manuf Sci 7:163
3. Hertzberg RW (1996) In: Deformation and fracture mechanics of engineering materials. John Wiley & Son Inc., USA, p 123
4. Humphreys FJ, Hatherly M (1995) In: Recrystallisation and related annealing phenomena. Pergamon, Great Britain p 12
5. Frigaard Ø, Grong Ø, Midling O (2000) Metall Mater Trans A 32A:1189
6. Robson JD, Sullivan A, Shercliff HR, McShane G (2004) In: Threadgill P (ed) Proceedings of the 5th international symposium on friction stir welding. TWI, Cambridge, Session 8B, Paper 2
7. Liu G, Murr LE, Niou C-S, McClure JC, Vega FR (1997) Scripta Mater 37:355
8. Jata KV, Semiatin SL (2000) Scripta Mater 43:743
9. Strangwood M, Berry JE, Cleugh DP, Leonard AJ, Threadgill PL (1999) In: Threadgill P (ed) Proceedings of the 1st international symposium on friction stir welding. TWI, Cambridge, Session 11, Paper 3
10. Biallas G, Braun R, Dalle-Donne C, Staniek G, Kaysser WA (1999) In: Threadgill P (ed) Proceedings of the 1st international symposium on friction stir welding. TWI, Cambridge, Session 3, Paper 3
11. Strangwood M, Davis CL, Attallah MM (2004) In: Threadgill P (ed) Proceedings of the 5th international symposium on friction stir welding. TWI, Cambridge, Session 8A, Paper 3
12. Threadgill P (1997) TWI Bull 38:30
13. Svensson L-E, Karlsson L, Larsson H, Karlsson B, Fazzini M, Karlsson J (2000) Sci Technol Weld Joining 5:285
14. Sato YS, Park SHC, Kokawa H (2001) Metall Mater Trans A 32A:3033
15. Sato YS, Sugiura Y, Kokawa H (2003) In: Threadgill P (ed) Proceedings of the 4th international symposium on friction stir welding. TWI, Cambridge
16. Sato YS, Urata M, Kokawa H, Ikeda K (2003) Mater Sci Eng A354:298
17. Sato YS, Sugiura Y, Shoji Y, Park SHC, Kokawa H, Ikeda K (2004) Mater Sci Eng A369:138
18. Rohatgi A, Vecchio KS (2003) Mater Sci Eng A328:256
19. Zhao YH, Liao XZ, Jin Z, Valiev RZ, Zhu YT (2004) Acta Mater 52:4589
20. Baker I, Liu L, Mandal D (1995) Scripta Metall et Mater 32:167
21. Chen SP, Vossenberg MS, Vermolen FJ, van de Langkruis J, van der Zwaag S (1999) Mater Sci Eng A272:250
22. Furukawa M, Horita Z, Nemoto M, Valiev RZ, Langdon TG (1996) Acta Mater 44:4619
23. Mahoney M, Mishra RS, Nelson T, Flintoff J, Islamgaliev R, Hovansky Y (2001) In: Jata KV, Mahoney MW, Mishra RS, Semiatin SL, Field DP (eds) Friction stir welding and processing. TMS, 183
24. Wang SC, Zhu Z, Starink MJ (2005) J Microscopy 217:174
25. Ashby MF (1971) In: Kelly A, Nicholson RB (eds) Strengthening methods in crystals. Elsevier, Amsterdam, p 184
26. Xu S, Deng X (2002) In: Proceedings of the 21st Southeastern Conference on Theoretical and Applied Mechanics (SECTAM XXI). p 699, Paper 2108
27. Attallah MM, Davis CL, Strangwood M (2005) In: Howe JM, Laughlin DE, Lee JK, Dahmen U Soffa WA (eds) Proceedings of the 5th international conference on solid-to-solid phase transformations in inorganic materials. TMS, 849